International Journal of Nanomedicine

Dovepress
open access to scientific and medical research

Open Access Full Text Article

ORIGINAL RESEARCH

Recovering Osteoblast Functionality on TiO_2 Nanotube Surfaces Under Diabetic Conditions

Benjamin Valdez-Salas[1], Sandra Castillo-Uribe[1], Ernesto Beltran-Partida[1], Mario Curiel-Alvarez[1], Oscar Perez-Landeros[1], Minerva Guerra-Balcazar[2], Nelson Cheng[3], Daniel Gonzalez-Mendoza[4], Olivia Flores-Peñaloza[1]

[1]Laboratorio de Biología Molecular y Cáncer, Instituto de Ingeniería, Universidad Autónoma de Baja California, Mexicali, Baja California, México; [2]Facultad de Ingeniería, División de Investigación y Posgrado, Universidad Autónoma de Querétaro, Querétaro, México; [3]Magna International Pte Ltd, Singapore; [4]Instituto de Ciencias Agrícolas, Universidad Autónoma de Baja California, Mexicali, Baja California, México

Correspondence: Ernesto Beltran-Partida, Laboratorio de Biología Molecular y Cáncer, Instituto de Ingeniería, Universidad Autónoma de Baja California, Blvd. Benito Juárez y Calle de la Normal, Mexicali, Baja California, C.P. 21280, México, Email beltrane@uabc.edu.mx

Introduction: Titanium (Ti) and its alloys (eg, Ti_6Al_4V) are exceptional treatments for replacing or repairing bones and damaged surrounding tissues. Although Ti-based implants exhibit excellent osteoconductive performance under healthy conditions, the effectiveness and successful clinical achievements are negatively altered in diabetic patients. Concernedly, diabetes mellitus (DM) contributes to osteoblastic dysfunctionality, altering efficient osseointegration. This work investigates the beneficial osteogenic activity conducted by nanostructured TiO_2 under detrimental microenvironment conditions, simulated by human diabetic serum.

Methods: We evaluated the bone-forming functional properties of osteoblasts on synthesized TiO_2 nanotubes (NTs) by anodization and Ti6Al4V non-modified alloy surfaces under detrimental diabetic conditions. To simulate the detrimental environment, MC3T3E-1 preosteoblasts were cultured under human diabetic serum (DS) of two diagnosed and metabolically controlled patients. Normal human serum (HS) was used to mimic health conditions and fetal bovine serum (FBS) as the control culture environment. We characterized the matrix mineralization under the detrimental conditions on the control alloy and the NTs. Moreover, we applied immunofluorescence of osteoblasts differentiation markers on the NTs to understand the bone-expression stimulated by the biochemical medium conditions.

Results: The diabetic conditions depressed the initial osteoblast growth ability, as evidenced by altered early cell adhesion and reduced proliferation. Nonetheless, after three days, the diabetic damage was suppressed by the NTs, enhancing the osteoblast activity. Therefore, the osteogenic markers of bone formation and the differentiation of osteoblasts were reactivated by the nanoconfigured surfaces. Far more importantly, collagen secretion and bone-matrix mineralization were stimulated and conducted to levels similar to those of the control of FBS conditions, in comparison to the control alloy, which was not able to reach similar levels of bone functionality than the NTs.

Conclusion: Our study brings knowledge for the potential application of nanostructured biomaterials to work as an integrative platform under the detrimental metabolic status present in diabetic conditions.

Keywords: osteoblast regeneration, bone surface interactions, cellular nanomodulation

Introduction

Orthopedic and dental implants have been successfully used for decades to replace or repair damaged bones, joints, and teeth.[1] However, many clinical biomaterials have shown limited functionality under local and systemic diseases,[2] that challenge the successful performance of metallic implants in terms of effective osseointegration, bone quantity and quality regeneration.[3,4] Thus far, DM is one of the most critical systemic diseases that negatively compromises the appropriate bone integration to the implant and the subsequent healing required for effective tissue restoration.[5,6] DM has been described as a group of metabolic disorders characterized by hyperglycemia caused by defects in insulin secretion, insulin action, or both.[7,8] Furthermore, DM is strongly associated with periodontitis, delayed wound healing, a high risk

Received: 2 September 2022
Accepted: 8 November 2022
Published: 18 November 2022

Graphical Abstract

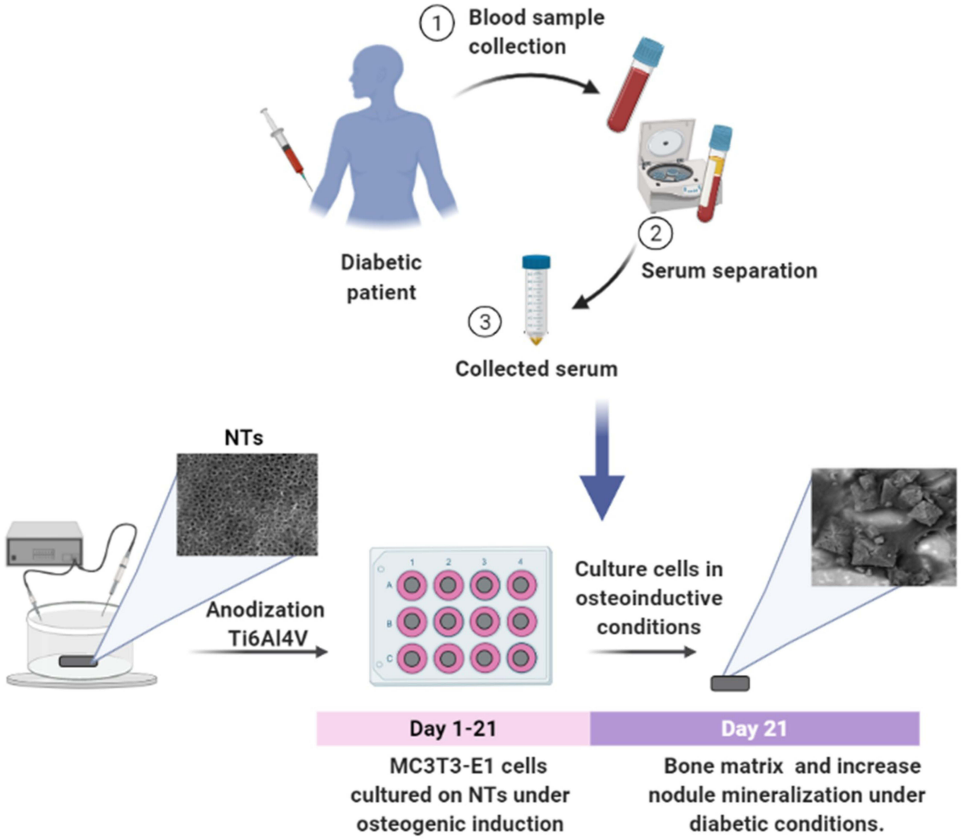

of infections, and, more severely, impairments of bone metabolism.[9–11] Concernedly, the current trends outline that DM type 2 accounts for ~ 85–90% of diagnosed patients who will require the application of implantable devices.[5] Interestingly, a recent retrospective study on implant failure showed that diabetes mellitus positively correlates with implant removal.[12] On the other hand, another retrospective work analyzing 742 dental implants showed a 4.50% failure rate between the control group (non-diabetic) and diabetic patients after the early stage of surgery.[13] However, one year after surgery, the researchers found an increase in implant failure to 9.82% in the diabetic group. Similarly, Olson et al reported an implant failure rate of 12% in diabetes mellitus patients,[14] which correlates with previous works, shedding light on the current need for innovative, groundbreaking metallic biomaterials to increase the survival rate.

Several studies have concluded that the microenvironment simulated using diabetic serum can result in poor osteoblast regeneration, decreased collagen synthesis, and improper matrix calcification.[11,15,16] Interestingly, the elevated glycosylated proteins, the autoxidation of glucose due to higher O_2^- levels,[17] and overproduction of reactive oxygen species (ROS) characterize the oxidative environment of the blood serum of diabetic patients.[18] Similarly, the expression of proinflammatory cytokines and mitochondrial oxidative stress have been outlined as constitutive factors of cellular damage in diabetic conditions.[19,20] Far more important is the negative impact of these biochemical and molecular components in the osseointegration process. Therefore, the correct osteoblast viability and functionality are impaired for rapid implant restoration. Hence, it is necessary to develop complementary therapeutic strategies, such as introducing metallic implantable materials with improved active surfaces.

Commercially pure Ti (Cp-Ti) and its alloys have been extensively selected as the primary option of metallic implantable devices for biomedical, orthopedic, and dental applications.[21–23] In this regard, Ti_6Al_4V alloy offers good

corrosion and fatigue resistance, and favorable mechanical properties compared to Cp-Ti.[22] Moreover, Ti_6Al_4V provides acceptable biocompatibility, osseointegration, osteoconductivity, bone-to-implant contact, and long-term success rates principally in patients without any metabolic disease.[24,25] Interestingly, the surface physicochemical parameters of metallic biomaterials have been widely described as playing a pivotal role in the control of cellular functionality. The current trends outline that nanostructured materials enhance the physicochemical properties, thus offering a versatile platform to promote cellular growth followed by tissue restoration.[24] For instance, nanomodified surfaces such as NTs of 70–100 nm diameter are described as a frontline strategy to orchestrate a favorable osteoblastic functionality, rapid proliferation, osteogenic expression, and maturation compared to their nonmodified counterparts.[22,24,26] Therefore, this essential information hypothesizes that NTs can stimulate osteoblast growth functionality under severe diabetic conditions.

In a previous study, Jiang et al suggested that sandblasted/acid-etched and anodized Cp-Ti surfaces improved the osteogenic expression and proliferation of MC3T3-E1 cells using high glucose levels (25.5 mM) as DM conditions.[27] Similarly, Yang et al reported that glucose simulating DM (22 mM) decreases the adhesion and the bone-forming performance of MC3T3-E1 on flat and SLA-modified Cp-Ti.[28] Meanwhile, the application of 80-nm diameter NTs supported osteoblastic proliferation and maturation after 21 days of evaluation. However, those interesting investigations are limited by only using glucose as a DM stimulus, despite the harmful DM environment involving more complex and detrimental substances that compose DM serum.

Therefore, considering the above-stated information and given the urgent need for novel metallic biomaterials supporting DM, the present study evaluates the beneficial properties of Ti_6Al_4V configured with ~70 nm NTs on osteoblast growth functionality using human DM serum for simulating the DM environment. Our current results advance the knowledge in the design of stimulating regenerative surfaces for applications of tissue engineering in clinical DM and underline part of the concerning mechanism.

Materials and Methods

Synthesis of TiO_2 Nanotubes

For the manufacturing of homogenous and reproducible 80-nm diameter NTs, we used a previously established protocol.[29–31] Briefly, Ti_6Al_4V disks (ASTM F-136, Supra Alloys Inc., Camarillo, CA, USA) 12 mm in diameter and 2 mm in thickness were polished by following a metallographic procedure (ASTM E3-11) using SiC emery paper (100−2000 grit) and 0.5 μm alumina to achieve a mirror finish. Next, the samples were cleaned in an ultrasonic bath (Branson CPXH 2800, Emerson Electric Co., SLMO, USA) with pure acetone, ethanol, and distilled water for 20 min each. Then, the samples were placed in a special 125-mL electrochemical cell and anodized using an electrolyte solution prepared with Microdacyn (Oculus Technologies, Guadalajara, JAL, MEX) supplemented with 10 mg/L NH_4F (Sigma-Aldrich, St. Louis, MO, USA) and 100 mg/L NaCl (Sigma-Aldrich, USA) at pH 6.8. Next, a potential of 20 V was applied for 5 min at room temperature (RT) using a DC power supply and a platinum mesh as a counter electrode. The anodized samples were cleaned for 20 min under bath sonication with distilled water to eliminate residues of fluoride salts, rinsed with isopropyl alcohol, and dried in a desiccator for 12 h. Importantly, all experimental specimens were sterilized using ultraviolet (UV) irradiation (285 nm UVB light source) for 30 min on each side inside a class II biosecurity cabinet.

Surface Characterization

The surface and cross-sectional morphology of the experimental samples were characterized by field-emission scanning electron microscopy (FE-SEM; Tescan LYRA 3, Brno, Czech Republic), taking images at 20 kV accelerating voltage, a working distance of 9.00 mm and the diameter of tubes was measured using top-view analyses with the Image J software (1.48v, NIH, USA).[32] The chemical composition of the material surfaces was assessed by energy dispersive X-ray spectroscopy (EDX) (Tescan LYRA 3, Brno, Czech Republic) using a silicon drift detector coupled to FE-SEM. The surface topography and roughness values were studied using atomic force microscopy (AFM; NX10, Park Systems, South Korea) equipped with an anti-acoustic box and an active vibration isolation table to prevent noises and vibrations that can affect the measurements. The AFM was configured with a PPP-NCHR (Park Systems) tip with force constant = 42 N/m, resonance

frequency = 330 kHz using the non-contact mode. The samples were fixed on a magnetic sampler holder using bi-adhesive carbon tape. The operation scan rate for all the samples was 0.5 Hz, with a Z-feedback set point of 3×10^3 and amplitude of 21.376×10^3 nm. The scan surface area was 2.5 μm^2. To provide the surface roughness differences between the NTs and Ti_6Al_4V, we provide the average roughness (Ra), the root mean square division (Rq), and kurtosis (Sku) values. The static water contact angle (WCA) of the NTs and Ti_6Al_4V surfaces was tested by depositing a 5 µL droplet of deionized water at 20 ± 2 °C and 45% relative humidity (RH). The droplet morphology was captured using a high-performance CCD camera of an automatized tensiometer (Theta Attension; Biolin Scientific) equipped with an X-Y syringe. The WCA results were obtained using the ONE Attension software, which enables a precise analysis of the two angles of the drop.

Human Serum Collection

After oral and written informed consent was obtained, blood was collected from three donors ranging from 40–60 years old: two women diagnosed with type 2 diabetes mellitus (DS1 and DS2) prescribed only with hypoglycemic drugs (metformin/glibenclamide), and a healthy male patient (HS) without any evidence of DM (Table S1). The blood samples were collected in the fasting state, and serum was separated by centrifugation at 3000 × g for 15 min and sampled inside a class II biosecurity cabinet. The serum samples were aliquoted and stored at −80 °C until used. It is important to highlight that FBS (Gibco-Invitrogen) was applied as the normal cellular control condition. The protocol for blood sample collection was approved by the bioethical committee from the Comité Nacional de Investigación Cientifica of Instituto Mexicano del Seguro Social, in compliance with the outlined in the Declaration of Helsinki.

Cell Culture

The initial preosteoblast mouse calvaria derived cell line MC3T3-E1 (ATCC CRL-2594) was cultured in α-minimum essential medium (α-MEM, Gibco-Invitrogen) supplemented with 10% FBS and 1% penicillin/streptomycin (Gibco-Invitrogen). The cells were incubated at 37 °C in a humidified atmosphere of 5% CO_2, and the medium was changed every 2–3 days after reaching an 80% confluence. To assess the cell proliferation, cytotoxicity, and morphology, each experimental sample was positioned in an individual well of a sterile 12-well polystyrene plate (Corning, NY, USA). Then, the cells were harvested and seeded on the specimens using 1 mL of medium containing a concentration of 1×10^4 cells/cm^2 for 24 h. Next, the medium was changed to medium supplemented with HS, DS of each DM patient or FBS as a positive control of osteoblastic growth. Each serum supplement was switched to 5% for each experimental time to maintain the cells under a quiescent state. The application of DS in this scheme attempt to mimic the pathophysiological conditions that occur in type 2 DM patients.[33] The use of HS from a normal non-diagnosed DM patient was selected as a control to mimic the normal human physiological condition.[34] The medium was changed every 3 days or after completing the required assays. The MC3T3-E1 cells were used between passages 3 and 6.

MTT Assay for Cell Viability

The cell metabolic activity was assessed with the 3-(4,5-dimethylthiazol-2-yl)-2,5-diphenyltetrazolium bromide (MTT) assay. After incubation for 1, 3, 5 and 7 days, the cells were rinsed thrice with warm 1X phosphate-buffered saline (PBS). One milliliter of MTT (Sigma-Aldrich, USA) in α-MEM (5 mg/mL) was added to each well and further incubated at 37 °C in a humidified 5% CO_2 incubator for 3 h. The resulting formazan crystals were dissolved after discarding the medium containing MTT, and the 12-well plate was transferred to an orbital shaker at 200 rpm and 37 °C with 500 µL of dimethyl sulfoxide (DMSO; Sigma-Aldrich, USA) for 20 min under dark conditions. Then, 100 µL of the dissolved crystals were deposited in a 96-well polystyrene plate (Corning, USA), and the optical density (OD) was measured at 490 nm using a microplate reader (Thermo Fisher Scientific, USA).[35,36]

Osteoblast Characterization by FE-SEM

To evaluate morphological changes in MC3T3-E1 cells seeded on the anodized materials, FE-SEM analysis was carried out as described by others.[25] After culturing for periods of 4 h, 24 h, and 21 days of seeding, cells grown on the samples were rinsed three times with PBS (5 min) and fixed in 2.5% w/v glutaraldehyde (Sigma-Aldrich, USA) buffered with 0.1 M sodium cacodylate (Sigma-Aldrich, USA) at 4 °C overnight, washed three times for 5 min in 0.1 M sodium cacodylate

buffer and postfixed with 2.5% glutaraldehyde for 2 h at room temperature (RT). The cells were dehydrated in a graded series of ethanol solutions (25%, 50%, 70%, and 100%) for 15 min at each concentration. Finally, the samples were sputter-coated with gold (10-nm gold layer) for 8 s and observed at 5 kV accelerating voltage. The image J software was used to compute the length and density of filopodia on the NTs under the different biochemical serum conditions.[37]

Osteoblast Differentiation Assay

In the osteoblast differentiation assay, the cells were seeded on the specimens (NTs, Ti_6Al_4V and polystyrene 12-well culture plates) at a density of 1×10^4 cells/mL and cultured for 5 days in complete culture medium. Then, the cells were cultured in osteogenic medium (α-MEM with 5 mmol/L β-glycerophosphate, 1 nmol/L dexamethasone, and 100 μg/mL ascorbic acid) supplemented in separate aliquots with FBS, DS1, DS2, and HS as previously described. Each culture condition was maintained by changing the corresponding medium twice per week until each evaluation period was reached.

Mineralization Assay

Bone matrix mineralization was determined by Alizarin Red S (ARS, Sigma-Aldrich, USA) staining of cultured osteoblasts to detect the deposited calcium nodules. Briefly, after osteogenic induction for 7, 14, and 21 days, the specimens were washed three times with PBS, fixed in 4% paraformaldehyde for 30 min at RT, rinsed thrice with PBS, and stained with 40 mM ARS solution (pH 4.2) in PBS for 20 min at RT. Then, the specimens were soaked with distilled water until the unbound stain was completely removed, dried in a desiccator and imaged using a professional digital camera (Nikon D750, NY, USA). ARS stain was dissolved from the cell matrix by incubating in 10% acetic acid at RT for 30 min. Then, the cells were collected in a microcentrifuge tube and heated at exactly 85 °C for 10 min. Briefly, the tubes were incubated on ice for 5 min, and the suspension was centrifuged for 15 min at 10,000 rpm. After centrifugation, the supernatant was transferred to a new tube, ammonium hydroxide was added to neutralize the acid, and the absorbance was measured at 405 nm in a microplate reader.[38] In order to calculate the concentration of ARS bonded to the mineralized samples, we performed dilutions of an ARS standard (40 mM) ranging between 2 mM and 0.0625 mM to allow measurement within the linear range of the assay.[38]

Collagen Secretion Assay

Collagen deposition on the anodized specimens in response to MC3T3-E1 cellular functionality was evaluated and quantified by the Sirius red staining-based colorimetric assay.[39] After osteogenic induction for 14 days as described, the specimens were rinsed three times with PBS, fixed with 4% paraformaldehyde for 45 min, rinsed three times with PBS, and stained with a 0.1% solution of Direct Red 80 (Sigma-Aldrich, USA) in aqueous saturated picric acid for 18 h at RT. After rinsing with 0.1 M acetic acid to remove the total unbound stain, the specimens were dried in a desiccator for 12 h. The samples were photographed using a professional digital camera (Nikon D750, NY, USA). Next, the stained specimens were eluted in 1 mL of the destaining solution (0.2 M NaOH/methanol 1:1) for 10 min, and the absorbance was measured at 570 nm using a microplate reader.

Immunofluorescence Staining

After 7 days for RUNX2 and 21 days for osteocalcin (OCN), osteopontin (OPN) and osteoprotegerin (OPG) the cells cultured on the anodized samples were washed three times with warm PBS and fixed with 4% paraformaldehyde for 45 min at RT. Once fixed, the cells were washed three times with PBS and permeabilized using 0.1% Triton X-100 in PBS for 30 min. Next, the samples were washed three times, incubated for 2 h at RT in bovine serum albumin (BSA) blocking solution (1% BSA/1 × PBS), and washed three times with PBS. Then, the cells were incubated for 2 h in primary antibodies against OCN at a 1:80 dilution (Abcam, Cambridge, MA, USA), OPN at a 1:1000 dilution (Abcam, Cambridge, MA, USA), RUNX2 at a 1:1000 dilution (Abcam, Cambridge, MA, USA) and OPG at a 1:200 dilution (Abcam, Cambridge, MA, USA) in blocking solution at 4 °C overnight. Then, Alexa Fluor 488-labeled antirabbit, 1:1000 dilution (Invitrogen, Carlsbad, CA, USA), and Alexa Fluor 594 labeled antimouse, 1:1000 dilution (Invitrogen, Carlsbad, CA, USA), each in blocking solution, were used as secondary antibodies for OCN, OPN, Runxs and OPG, respectively,

incubated for 2 h at RT and washed three times with PBS.[29] The cell nuclei were counterstained using 4′,6′-diamidino -2-phenylindole (DAPI) (Molecular Probes, Carlsbad, CA, USA) in PBS, incubated for 20 min at RT, and washed three times with PBS.[27] Finally, the surfaces were inverted onto coverslips with fluorescence mounting medium (Fluroshield, Sigma–Aldrich, USA), examined, and photographed using a green (OPN, Runxs and OPG), red (OCN), and blue (DAPI) filter employing a fluorescence microscope under similar magnifications. To measure the fluorescence intensity, 5–10 micrographs of each sample were taken at the corresponding culture period using the same exposure time. The average intensity was measured using ImageJ software from five random cells on each surface.

Statistical Analysis

At least three independent experiments were performed, each in triplicate. Statistical analysis was performed using one-way analysis of variance (ANOVA) followed by Bonferroni's multiple comparison test for multiple group comparisons using GraphPad Prism 6 software (Graph Pad, CA, USA). A $P < 0.05$ was considered statistically significant. The results are expressed as the mean ± standard deviation (SD).

Results

Surface Analysis

Figure 1 shows the surface structural morphology of the experimental materials, characterized using FE-SEM. The anodization process results in the formation of a highly ordered nanoconfigured TiO_2 layer with a wall width of 83 ±13 nm and a layer thickness of 1.18±0.01 µm (cross-section view) formed on the whole surface of the Ti_6Al_4

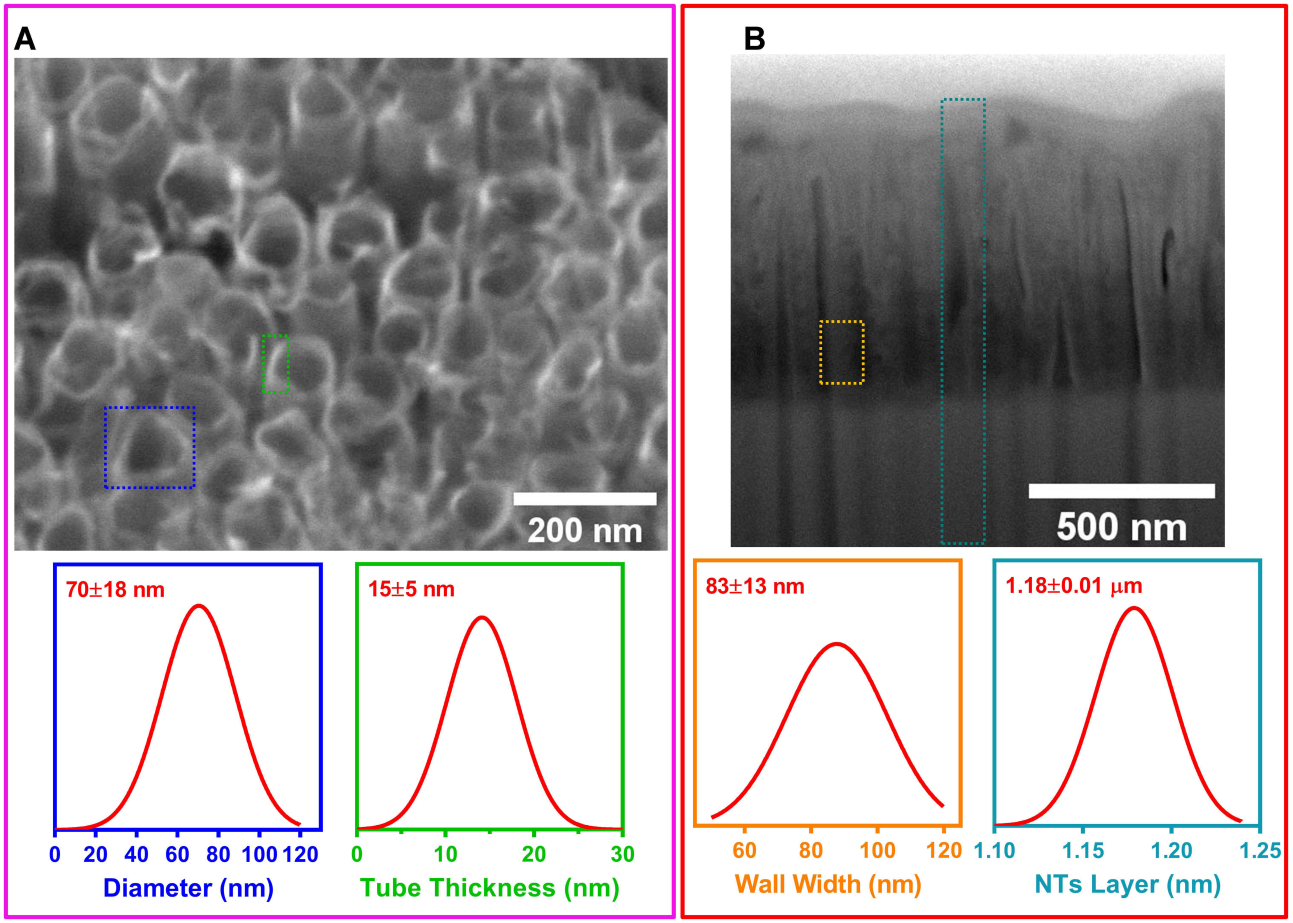

Figure 1 FE-SEM analysis of the anodized NT surface. (**A**) Top-view micrograph of NTs showing the diameter and tube thickness distribution. (**B**) Cross-section view of the NT layer illustrating the wall width and layer broadness.

V specimens. Moreover, the AFM analysis showed the transformation of the flat non-anodized Ti_6Al_4V control alloy (Figure 2A) to a uniformly nanostructured surface (Figure 2B). Furthermore, the Ra (Figure 2B) and Rq (Figure 2C) values displayed an exorbitant roughness increment after the anodization. Similarly, the topography distribution illustrated a flattened profile from the Ti_6Al_4V, which was promptly spiked after the synthesis of the NTs (Figure 2D). This approach further supports the presence of homogeneous, well-aligned, rougher and uniformly distributed NTs over the modified sample. The NTs were estimated to have a tube diameter of 70±18 nm and a mouth thickness of 15 ±5 nm (top view). On the other hand, the surface hydrophilicity was significantly increased after the anodization, showing a decreased WCA for the NTs (Figure S1).

Effect of Human Serum on Osteoblast Viability

The impact of the different simulated microenvironments using human serum on the viability and proliferation of MC3T3-E1 cells on the NT surfaces was evaluated by MTT assay (Figure 3). MTT indicates the differences between the proliferating cellular rate on the NT surface under DM, human serum and FBS conditions. The results highlight that the initial cellular viability was similar between the experimental conditions. However, at Day 3, higher proliferation was observed under the experimental conditions than on the first day, and prominent growth was observed with FBS, which followed this similar behavior after 5 days of incubation. Moreover, after 7 days, we detected that the nanoconfigured materials were capable of maintaining late osteoblast activity; thus accentuating the DM conditions attenuated by the

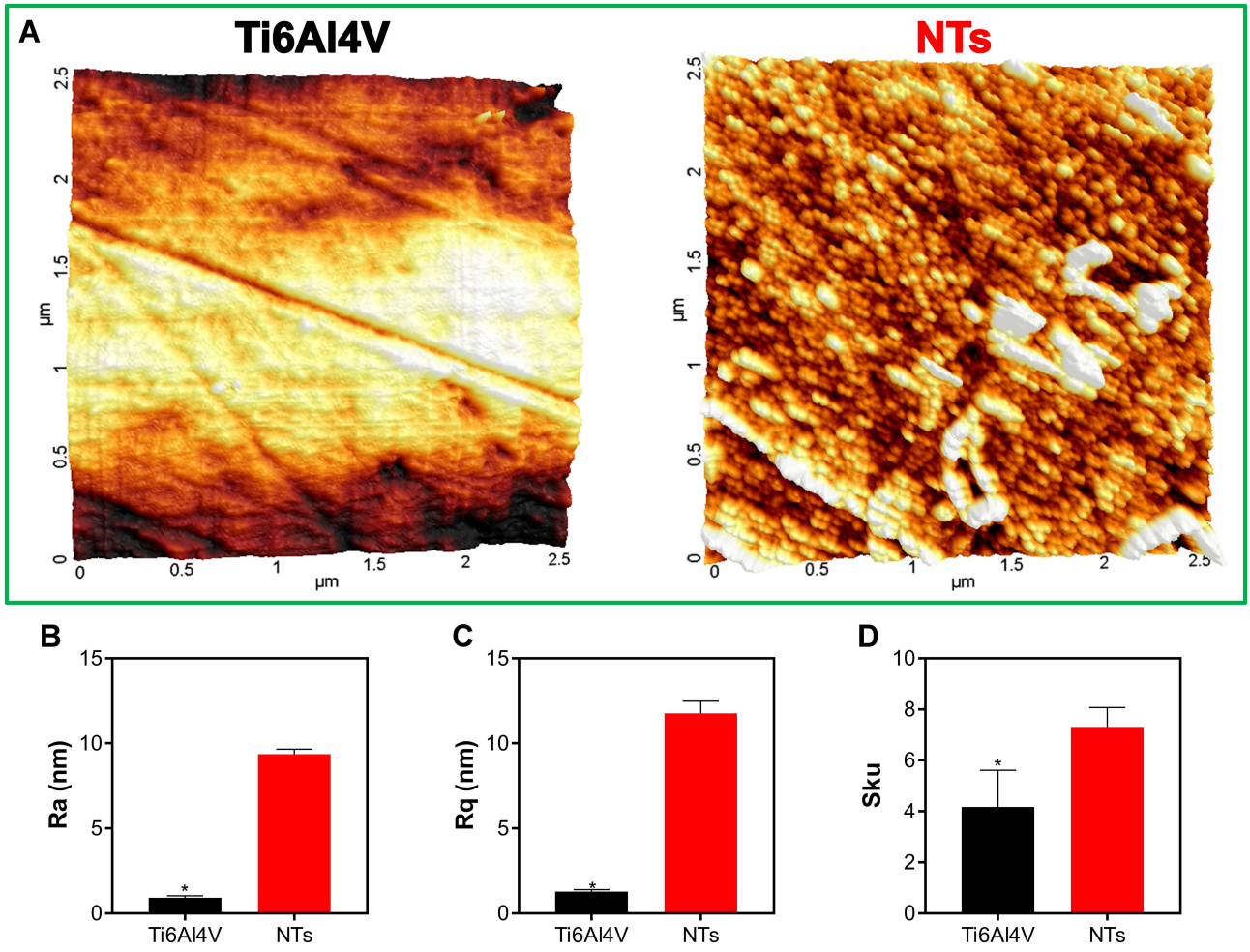

Figure 2 AFM analysis of the Ti_6Al_4V control surface and the NTs. (**A**) 3D micrographs showing the surface topography. (**B**) Ra values of the experimental materials. (**C**) Rq data of the surfaces. (**D**) Sku of the obtained from the surface characterization. The * shows significant differences.

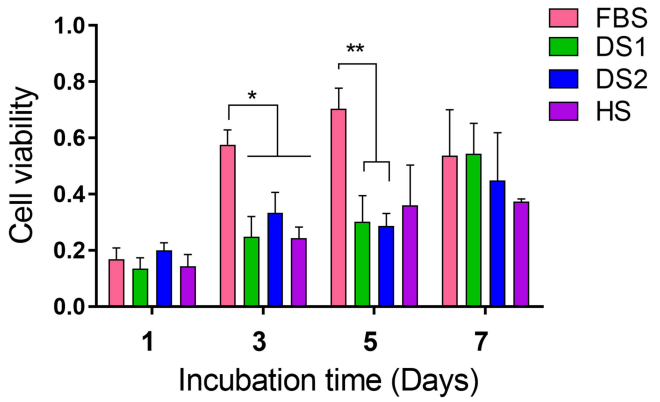

Figure 3 MTT assay showing osteoblast viability under the experimental conditions after 1, 3, 5, and 7 days of incubation. * and ** indicate significant differences between serum conditions.

presence of proliferating cells (Figure 3). It is important to highlight that the DS and HS groups did not show significant differences.

MC3T3E-1 Adhesion and Morphology

To study the cell morphology of the specimens and biochemical environments, we used FE-SEM technology. Initially, Figure 4 shows the morphology of MC3T3-E1 adhered to the NTs for 4 h. The low magnification micrographs showed that a promoted cell spread was stimulated by the controls (as expected) compared with the DS1 and DS2 conditions. However, the NTs exhibited an evident cellular distribution, showing a typical osteoblastic shape with a dense ECM; cytoplasmic prolongations and well-defined filopodia were detected among the different biochemical conditions. Moreover, the application of the different medium conditions resulted in a controlled filopodia extension and density (Figure S2), suggesting that the nanotopography could be the initial factor directing the front line of cell adhesion.

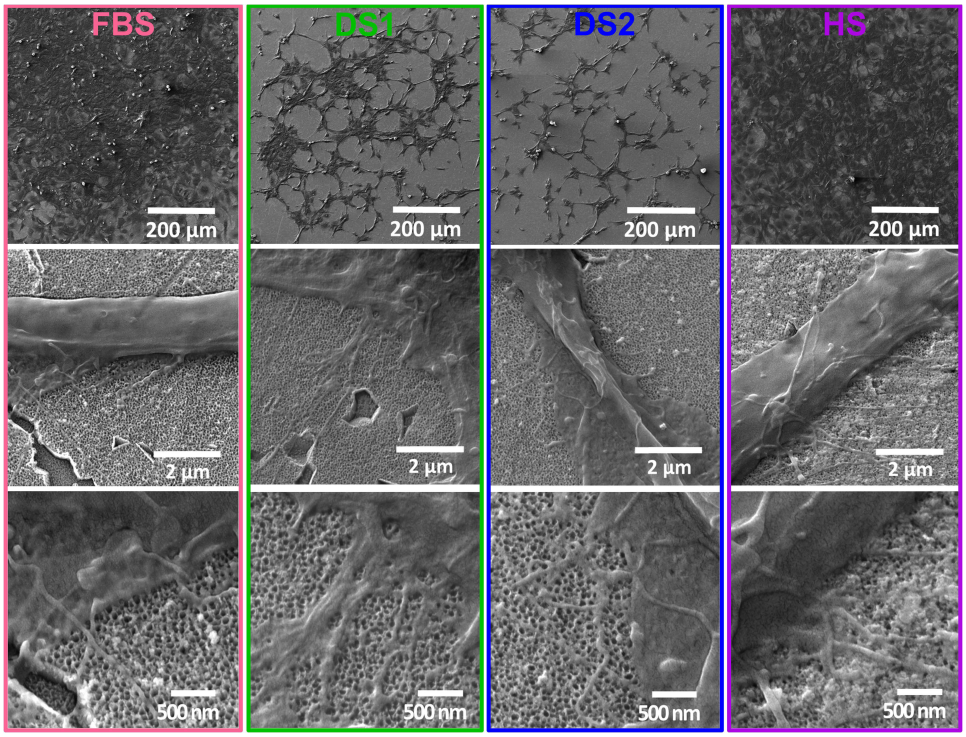

Figure 4 FE-SEM micrographs illustrating the osteoblast adhesion and cell morphology on the NTs after 4 h of culture. Magnifications are 250 X, 30,000 X and 80,000 X.

Therefore, the NTs harbor attachments with other cells. The magnified images illustrated well-defined extending lamellipodia and filopodia on all surfaces under biochemical conditions. Furthermore, the longed, abundant and pronounced finger-like fibrillar shaped protrusion extending from the cell body, embracing, and interacting with the nanotopography highlights a strong cell adhesion, accelerated by the NTs.

After 24 h of incubation (Figure 5), homogeneous cellular spreading over the NTs was evident in the experimental microenvironment. Thus, abundant cytoplasmic prolongations maintain and promote cell attachment, clear cell bodies, a denser ECM and the extension of the bone monolayer. However, the DS2 showed a decreased cellular elongation compared to the experimental conditions (Figure S2). Thus, 24 h of culture could be a reasonable period for initial cellular sensing of the adverse molecular microenvironment stimulated by the DS. The higher zoom displayed outstanding filopodia that were efficiently anchored, thus tailoring osteoblast adhesion and proliferation.

Osteoblast Differentiation

Osteoblasts give rise to bone formation through cell proliferation, differentiation, and extracellular matrix mineralization. The calcium (Ca) formation and deposition from the growing osteoblasts were quantitatively assessed using the ARS staining assay. Interestingly, Figure 6A and B illustrate the results of ARS analysis of MC3T3-E1 cells cultured on the NTs and the Ti_6Al_4V control surface (FBS, DS1, DS2, HS) after osteogenic differentiation for 7, 14 and 21 days. Initially, Figure 6A displays the surface materials with a red color shade increasing in intensity and uniformity from 7, then 14 and 21 days of differentiation. Moreover, we detected that the formation of calcified nodules was constantly stimulated by the NTs in the different biochemical conditions, and in comparison with the Ti_6Al_4V materials, thus highlighting a similar mineralization behavior. The results obtained from ARS quantification represent a remarkably similar trend from the initial to middle phase of maturation between the different media completed with the experimental sera (Figure 6B). However, an exacerbating significant ARS quantity was appreciated in the late osteoblastic differentiation phase (21 days) for the NTs, further indicating a higher and evident nodule formation for the simulated microenvironment. Furthermore, it was clearly detected that the nanostructured surfaces promoted a faster initial bone mineralization, which was significantly higher in the late stage. Figure 7 a shows the collagen secretion from the

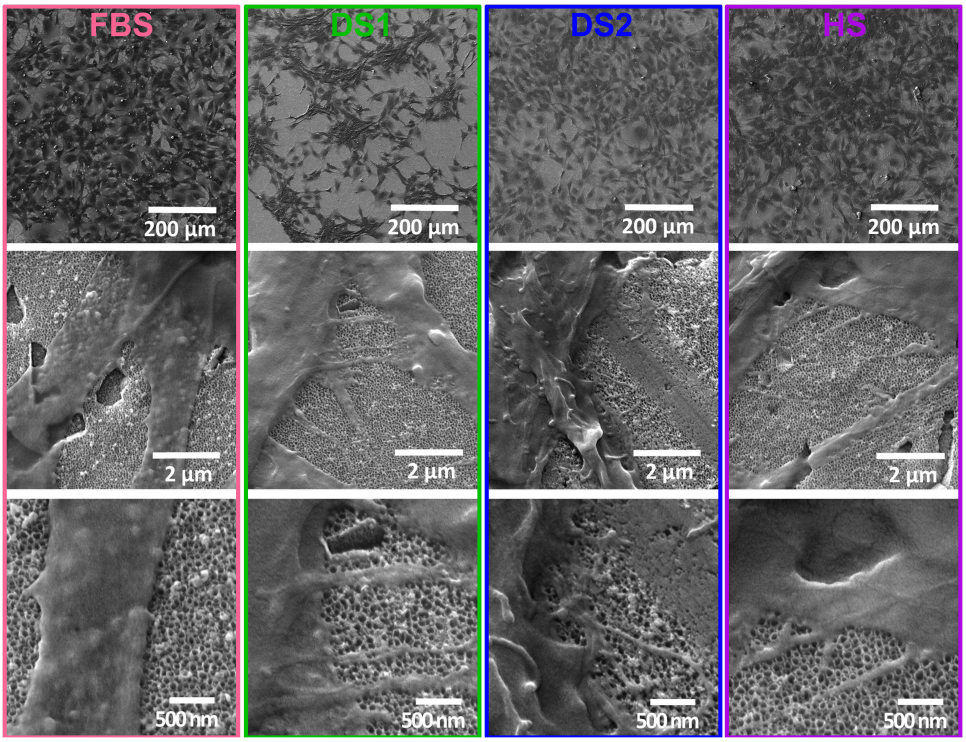

Figure 5 FE-SEM micrographs illustrating the osteoblast adhesion and cell morphology on the NTs after 24 h of culture. Magnifications are 250 X, 30,000 X and 80,000 X.

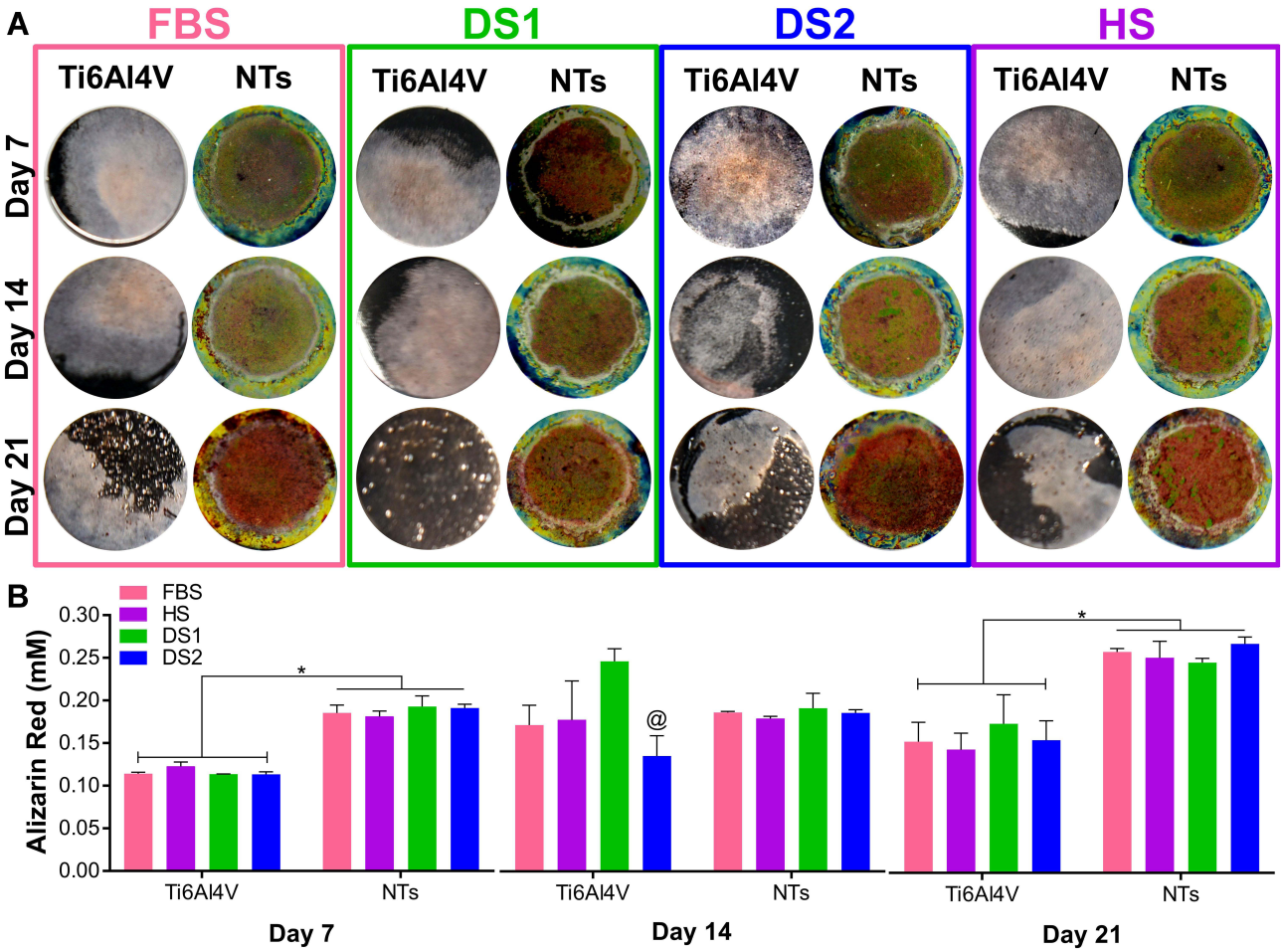

Figure 6 ECM mineralization and collagen secretion assay after osteogenic differentiation. (**A**) Mineralized nodules of Ti_6Al_4V and NTs stained with Alizarin red S (ARS), after 7, 14 and 21 days of differentiation. (**B**) Quantitative analysis of ARS staining on the surfaces. *Indicates significant differences in the ARS quantified between the Ti_6Al_4V and NTs. @ Represents changes between DS1 and the analyzed serums in Ti_6Al_4V after 14 days of incubation.

MC3T3E-1 cells stimulated by the nanoconfigured surfaces after 14 days of culture. Interestingly, a monolayer of cells stained by Picrosirius Red was detected. Of particular interest is collagen synthesis, which was closely similar among the simulated DM environments and serum controls. However, a slight collagen reduction was detected for the DS model, but no significant differences were calculated (Figure 7B). Therefore, the results of extracellular matrix mineralization are remarkably comparable to the results of collagen secretion.

FE-SEM Characterization of Differentiated MC3T3-E1 Cells

Figure 8A shows FE-SEM micrographs of MC3T3-E1 cells cultured on the NTs after osteogenic differentiation following 21 days of incubation. The lower magnification images show the distribution of the cells, highlighting the capability to extend among the NTs under the biochemical conditions (SBF, HS, DS1 and DS2). Moreover, the nanostructured surface promoted the secretion of well-defined hydroxyapatite crystals (Haps) on the cellular surface. Interestingly, the crystal secretions were detected mainly over the cellular bodies and in the close surrounding space, further supporting the results of ARS quantification (Figure 6B). The higher magnifications revealed the presence of abundant and large bone nodules produced by the osteoblastic cells that were stimulated even under detrimental conditions (by DS). These data correlated with the ARS results, indicating that NT surfaces promote and induce ECM mineralization, Ca accumulation, and nodule formation even under detrimental diabetic conditions.

EDX analysis was performed to evaluate the chemical composition of the ECM of the differentiated cells, as well as to estimate the atomic Ca and P levels by the experimental conditions. Figure 8B shows the percentage of Ca secreted by

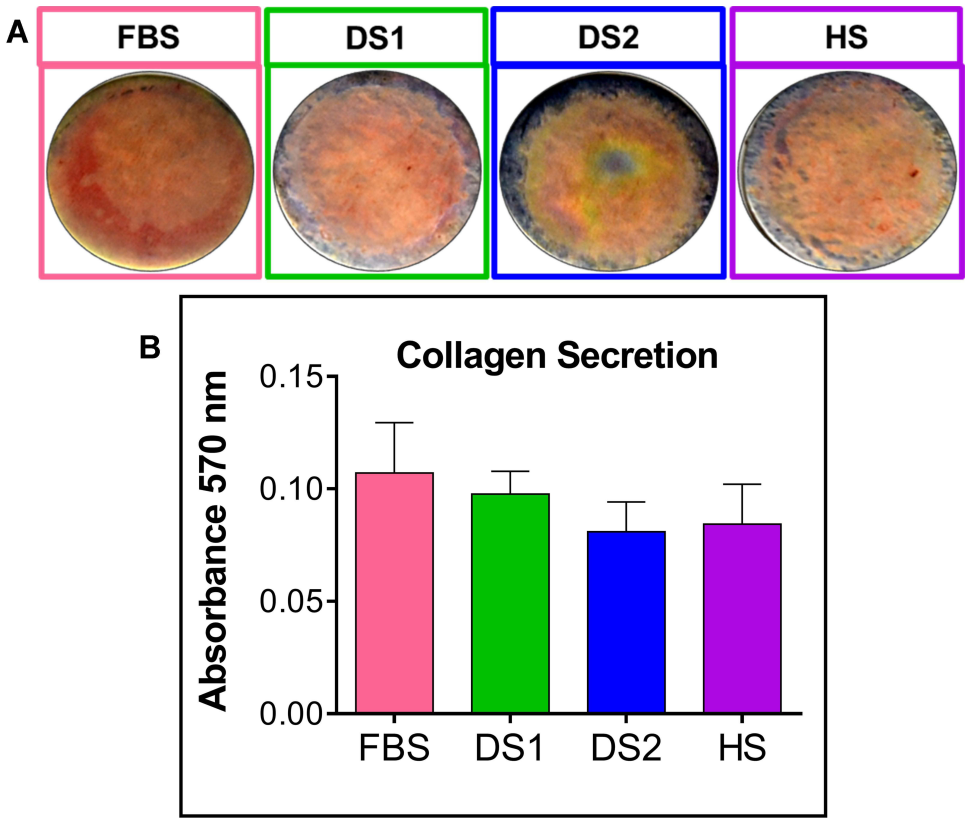

Figure 7 (**A**) Collagen secretion assay for 14 days of culture. (**B**) Quantification of secreted collagen.

the mature osteoblasts. The results showed that the positive control promoted Ca deposition more than the detrimental biochemical stimulus. However, the P composition was slightly lower in the DS conditions, but those differences were not significant (Figure 8C). Furthermore, the FE-SEM micrographs in Figure S3 support the formation of well-defined Hap crystals growing from the cellular bodies under the experimental conditions. Thus, the results suggest a consistent formation of Hap under harmful DM conditions. Interestingly, these results highlight that bone nodule formation was stimulated by the NTs under the different experimental conditions, suggesting a slightly promoted deposition of bone matrix minerals in the FBS, as expected.

Immunofluorescence Staining

To determine whether the biochemical conditions FBS, DS1, DS2, and HS modulate osteogenic expression, the osteoblast differentiation markers Runxs2, OCN, OPN, and OPG were assessed at 7 and 21 days of induction. Figure 9A shows the expression of Runx2 on the NTs under the experimental environments after 7 days of incubation. The cellular morphology induced by the serum treatments was similar. Moreover, Runx2 was detected principally around the nucleus for all the experimental environments (Figure 9A). To accurately assess and compare any significant differences between the biochemical stimuli, a representative graph of Runx expression is provided (Figure 9B). We detected a slight increase in the expression of DS1 in comparison to the studied sera; however, the differences were not significant. This information suggests that Runx2 expression can be supported in the early stage of osteoblastic differentiation even under detrimental DS. Moreover, the receptor expression of OCN was analyzed and quantified (Figure 10). In Figure 10A, the OCN staining suggests that the OCN was intracellularly localized mainly in the cytoplasmic space. The fluorescence quantification (Figure 10B) suggested that late osteogenic differentiation followed a similar activation behavior among all the experimental conditions (FBS, DS1, DS2 and HS). Similarly, OPN expression followed a similar pattern of activation (Figure 11B), suggesting that PG was also localized in the intracellular space (Figure 11A). The OPG receptor, a negative regulator of osteoclastogenesis, was intracellularly expressed, showing

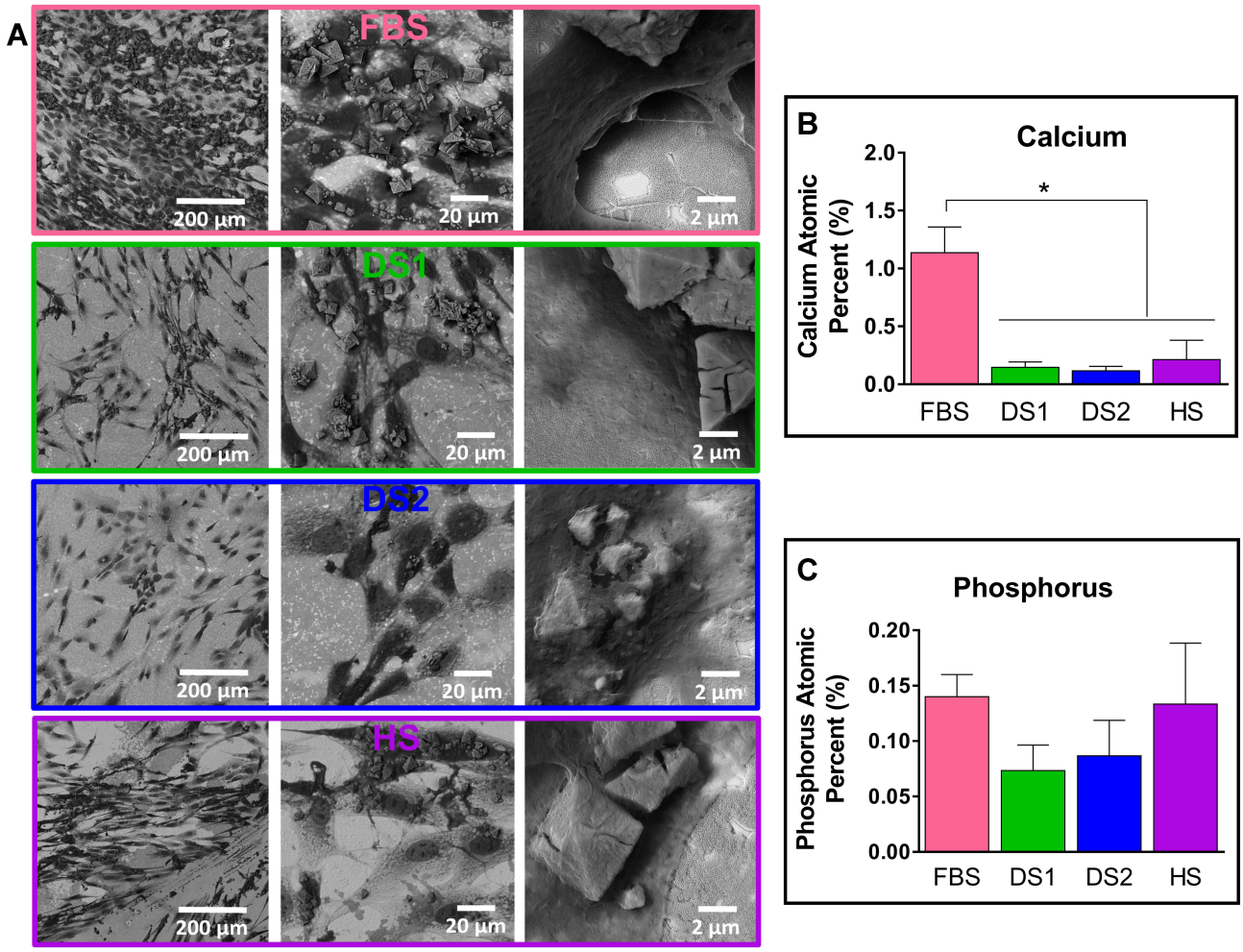

Figure 8 Hydroxyapatite nodule formation after osteogenic incubation for 21 days under the experimental conditions. (**A**) SEM micrographs showing abundant and large bone nodules on the NTs. Magnifications are 300 X, 1500 X and 15,000 X. (**B**) EDX analysis of the calcium atomic level. (**C**) Phosphorus atomic level secreted on the NTs. The *indicates significant differences.

a similar localization behavior for all the experimental conditions (Figure 12A). Interestingly, Figure 10B illustrates similar outcomes of OPG levels between FBS and the experimental serum microenvironments. However, DS2 and HS showed slight differences in reduced expression compared with DS1 (Figure 12B).

Discussion

The surface of implant materials must contribute physicochemical properties beneficial for the patient. These characteristics are a low elastic and fatigue modulus, excellent corrosion resistance, chemical stability, biocompatibility, and, more importantly, successful bone-to-implant integration (eg, osseointegration).[40] The osseointegration process demands efficient osteoblast adhesion, proliferation, secretion of EMC proteins, and mineralization of the surface of the material.[21] Interestingly, anodized Ti_6Al_4V with NTs improves osteoblast bone-forming functionality more than its nonmodified counterparts.[22,26,41] Moreover, we reported that NTs improved the angiogenic response compared with nonmodified flat Ti_6Al_4V, Cp-Ti, and rough acid-etched Ti_6Al_4V surfaces under standard culture conditions.[29] However, the requirement of metallic implants by older and metabolically compromised populations is still growing day-to-day.[42,43] Extensive evidence indicates that chronic DM impairs osteoblast cellular functionality (eg, proliferation, differentiation, mineralization).[5,15] Thus far, DM suppresses the bone mineral apposition rate, bone-to-implant contact, demanded osseointegration, and peri-implant bone formation.[11,44] Hence, it is imperative to develop and study novel nanostructured surfaces that can support and stimulate the formation of new bone under challenging conditions, such as

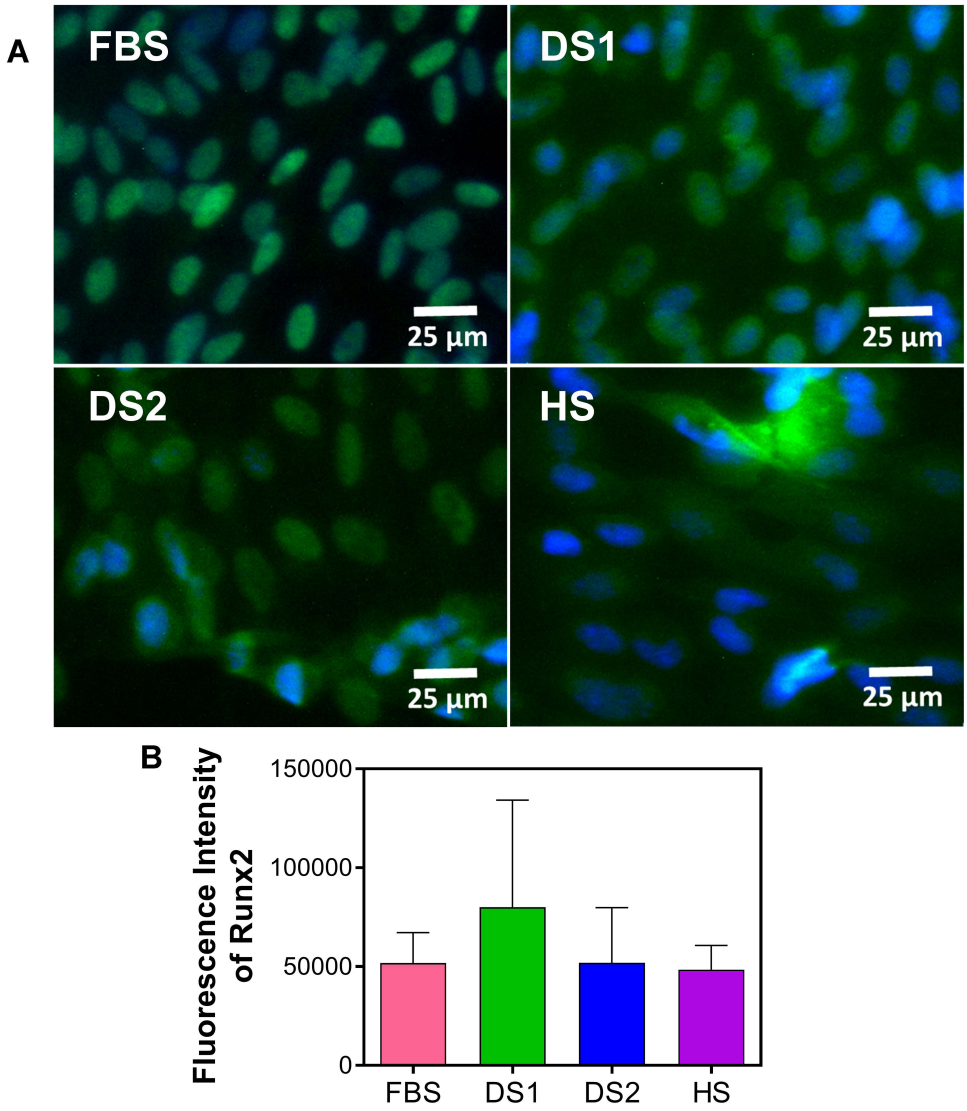

Figure 9 Immunofluorescence of Runx2 expression in MC3T3-E1 cells cultured for 7 days under the experimental conditions. (**A**) RUNX 2 intracellular localization, magnification is 20 X. (**B**) Graph representing the fluorescence intensity expressed for Runx2.

the DM environment. Therefore, this study focuses on characterizing osteoblast bone-forming capability by 70 nm Ti_6Al_4 V-NTs under the detrimental growing environment stimulated by diabetes mellitus (DM).

The anodization process is a successful method to synthesize NTs to improve the physicochemical and osteoblast growth functionality of Ti-based metallic implants.[21] Our current synthetic strategy resulted in the formation of homogenous, aligned, rougher, hydrophilic and uniform NTs, highlighting a coating thickness of 1.18 µm (Figure 1). It is important to outline that thicker nanostructured oxide coatings can improve the corrosion resistance and durability of Ti-based materials.[45–49] Moreover, the nanoconfigured structures can regulate and enhance the biological properties of implant surfaces, thus far proposing that osteoblast cellular activity can be performed even under adverse metabolic conditions.[6,50–52] Our present study indicates that early osteoblast growth performance (Days 3 and 5) is altered under diabetic serum conditions. However, after seven days, the proliferative activity reached similar outcomes for the studied conditions. These results suggest that DS boosts initial detrimental activity; nonetheless, NTs may develop a beneficial microenvironment in part by the higher controlled interconnecting nanorough and wetter surface that ameliorates the effects of DS, creating a prominent microenvironment that improves cell adhesion, following bone adaptation and subsequent late cellular regeneration. Interestingly, Jiang et al reported the proliferation of MC3T3-E1 cells on SLA and

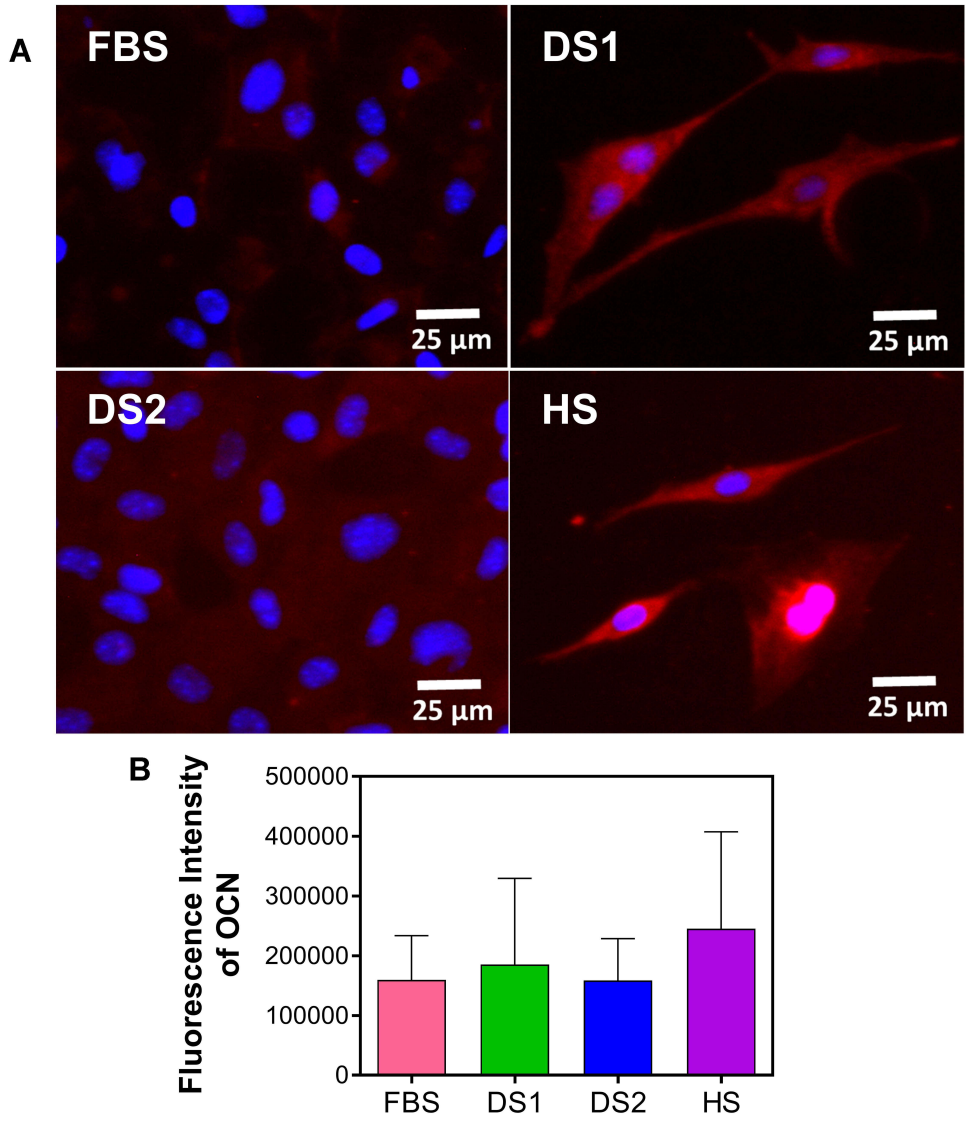

Figure 10 Immunofluorescence of OCN expression in MC3T3-E1 cells cultured for 21 days in conditioned serum. (**A**) OCN detection on the NTs, magnification is 20 X. (**B**) Graph showing the fluorescence intensity expressed for OCN.

anodized SLA surfaces cultured with normal serum and DS.[27] The authors detected that although SLA modifications dramatically increase the surface roughness, that reached an osteoblast proliferation rate similar to those rates witnessed in our current work. These interesting trends suggest that the nanoconfiguration parameters (surface area-to-volume, Ra, Rq, Sku) may play a pivotal role compared to a high roughness to promote bone proliferation under DM conditions. Moreover, in part, we can explain that NTs are interconnecting networks with a high surface area, aligned with each other orchestrating a sustainable microenvironment due to the easy transport of nutrients, growth factors, and biochemical signals for bone proliferation and maturation.[26,53] However, we need to consider that MTT is substantiated in mitochondrial health and activity, therefore supporting that osteoblast-NT contact interactions can ameliorate the energetic activity of DS effects, as proposed here (Figure 3).

It is important to highlight that the initial bone adhesion is required for conducting bone-surface contact interactions, activation of signaling pathways associated to proliferation and subsequent bone regeneration.[54,55] Therefore, we applied FE-SEM after the initial adhesion phase (4 h) and continuous late adhesion (24 h) to characterize the new bone formation conducted by our NTs (Figures 4 and 5). Interestingly, our work reveals that NTs could promote striking filopodia anchoring under DS conditions, illustrating the presence of thick networking extending cellular protrusion following the

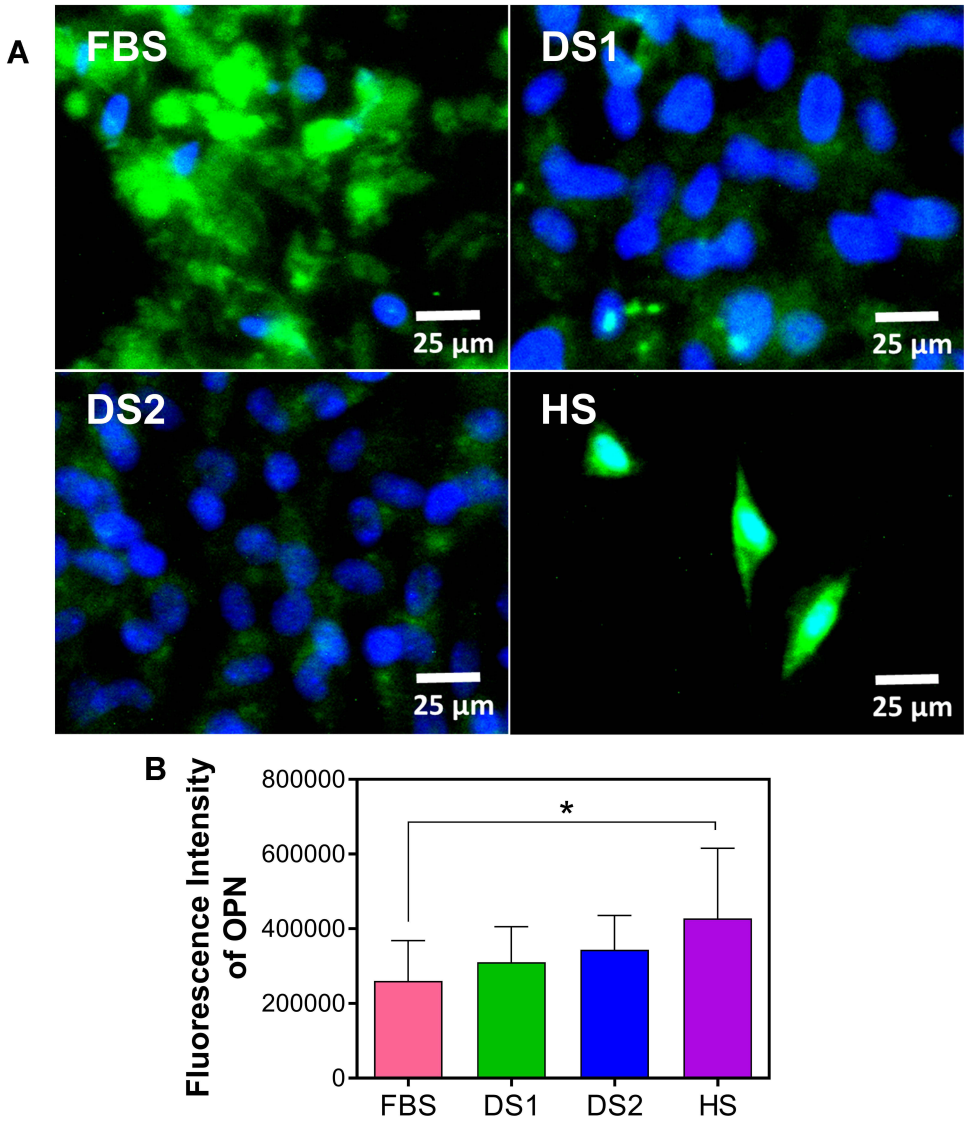

Figure 11 Immunofluorescence of OPN expression in MC3T3-E1 cells cultured for 21 days in the evaluated serum environments. (**A**) OPN detection after each treatment condition, magnification is 20 X. (**B**) Graph representing OPN fluorescence. The *indicates significant differences.

NT mouth structures. Moreover, the elongated cellular projections to the generation of a bone-forming monolayer coat the NTs, with continuous cell-cell interplay extending among the surface. A previous study reported that osteoblasts growing with DS showed a disrupted cellular morphology and stressed metabolism after 24 h of incubation.[34,56] However, the authors showed that isolating Ti with a hydroxyapatite (HA)/chitosan composite coating could ameliorate the aberrant cell configuration conducted by the DS.[56] Moreover, Li et al suggested that osteoblasts cultured under DS on porous Ti surfaces follow a detrimental, flat, poorly elongated cellular morphology with reduced protrusions accompanied by decreased bonding filopodia.[57] However, the application of a chitosan coating alleviated the aberrant morphology observed on the micron-porous Ti after eight days of incubation. This information suggests that our nanostructured surface can potentiate osteoblast adhesion behavior without utilizing expensive modification techniques. Of particular importance, the present study additionally suggests that diabetic serum conditions can promote osteoblast damage and reduce early cellular adhesion.

Extracellular matrix (ECM) mineralization is a critical process demanded during bone regeneration and bone-to-implant maturation. However, several studies have concluded that diabetic conditions can impair or, in the worst case, avoid successful bone mineralization.[44,58] Given the importance of promoting osteoblast functionality, we tested the

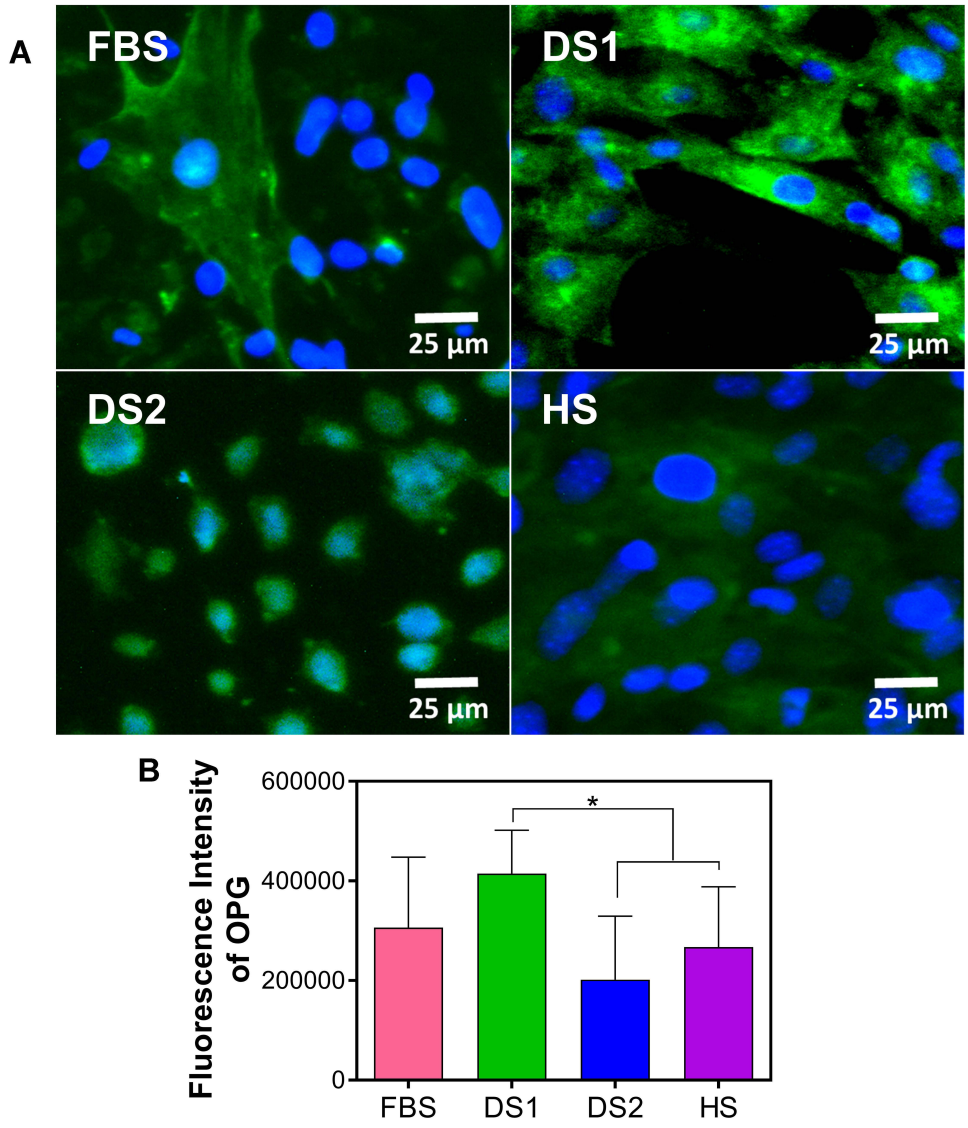

Figure 12 Immunofluorescence of OPG expression in osteoblasts cultured for 21 days in diabetic and control serum. (**A**) OPG intracellular detection, magnification is 20 X. (**B**) Graph illustrating the fluorescence intensity expressed for OPG. *Denotes significant differences between DS1 versus DS2 and HS treatment.

differentiation and, far more importantly, collagen secretion and bone-matrix mineralization conducted by the NTs under DS conditions. Our study demonstrates that the NT surface can support osteoblast bone-forming functionality at outcomes similar to those of using FBS, following substantial Ca/P elemental formation and collagen secretion. Indeed, it proves that the DS condition initially gives rise to detrimental cell proliferation; nonetheless, the NTs can develop a versatile scaffold that harbors a beneficial osteogenic environment. Far more importantly, the NTs further established an immediate and long-lasting maturation process than the nonmodified Ti_6Al_4V alloy, a significant step forward in the benefits of NTs. Several works have demonstrated that NTs from 70–100 nm can prominently increase bone mineralization performance.[21,22,59] Moreover, the application of nanoscale-featured surfaces can improve the focal adhesion kinase (FAK) signaling pathway, resulting in improved cellular adhesion and subsequent osteoblast mineralization and even angiogenic behavior.[29,60] Ma et al suggested that the reactivation of FAK phosphorylation with the subsequent integrin subunits α2, β1, and β3 expression by a nanoHA-Ti coating consequently reversed the suppression of the BMP-2/Smad pathway under DS.[61] The reported results indicated that osteogenic expression was recovered, accompanied by improved cellular adhesion and proliferation. Moreover, osteoblasts cultured in DS over Ti_6Al_4V coated with chitosan promoted the activation of the PI3K/AKT signaling system.[57] The authors used specific inhibitors

to propose that the deposited coating exerted an antioxidant action, immediately reducing the overproduction of ROS. Furthermore, a recent study of Ti_6Al_4V porous materials coated with silk fibroin illustrated that the osteoblast mineralization rate resists the adverse effect of DS after 14 days under DS incubation.[62] Interestingly, the authors advocated that promoted ROS associated with DS inhibited the activation of the NF-κB pathway, which led to an extended-lasting detrimental osteoblast functionality and increased cellular apoptosis. Nevertheless, those works have required the application of different composite materials to ameliorate the cellular havoc conducted by DS. Meanwhile, our NTs have demonstrated similar outcomes of protective osteoblast functionality in a diabetic environment, probably promoting the accumulation and amplification of ions and biomolecules (which has been linked to the upregulation of calcium deposition) as well as integrin activation on the hydrophilic and nanorougher surface.[50] However, Yang and collaborators reported that NTs of 80 nm alleviated osteoblast behavior under the hazardous diabetic condition of DM simulated using only high glucose levels (22 mM).[28] Therefore, despite these results being in line with our current study, it is important to highlight that it is not equivalent to simulating DM using high glucose instead of DS. We consider that the overexpressed detrimental properties of DM result from the synergistic action between high glucose, DS-related proteins and inflammatory cytokines.[18,61] On the other hand, different molecular and drug substances may influence the biochemical behavior of human diabetic and healthy serums. Indeed, diabetic drug therapies (eg, Metformin) or biochemical modulators such as ascorbic acid can stimulate the osteoblast bone-forming functionality.[63–65] However, in our present study, we can highlight that the bone mineralization rate guided by the experimental surfaces (NTs and Ti6Al4V) followed a similar growth rate in terms of the evaluated human serum conditions and cellular control of FBS (Figure 6). Thus, proposing that the drug therapy of the selected patients may not interfere in the beneficial effects of the NTs.

To determine the effects of DS on osteoblast differentiation, the relative expression of the key osteogenic markers Runxs2, OCN, OPN, and OPG was evaluated. Interestingly, Runx2, an essential transcription factor that participates in the early osteogenesis rate, is considered an initial master gene for several genetic expression pathways in the early stages of osteoblast differentiation and upregulates OCN, the major structural component of the bone matrix.[66,67] In our investigation, immunofluorescence staining of Runx2 expression was performed on the surfaces of the experimental NTs at seven days of differentiation. The results indicated that the NTs tolerated the detrimental DS effects, thus inducing osteogenesis behavior similar to the behavior observed in the control culture conditions (FBS). Moreover, OCN showed similar outcomes of intracellular expression, further supporting that NTs stimulate the osteogenic late differentiation rate. Importantly, OCN and OPN are the most abundant noncollagenous bone matrix proteins that have crucial involvement in the initial bone matrix mineralization stage and are commonly considered an early marker of osteoblastic differentiation.[68] For this reason, we evaluated OCN and OPN expression at 21 days under these challenging conditions. Furthermore, we quantified OPN (a late osteogenic differentiation marker) after 21 days, illustrating the hallmarking outcome of sustained expression.[66] OPN plays a vital role during the biomineralization phase, including increasing bone cell adhesion by concentrating in the mineralized collagen matrix during bone tissue formation and modulating matrix mineralization.[69] However, OPG, which has an inhibitory action on the TNF receptor family, inhibits NF-κB and suppresses the RANK pathway, modulating the harmful environmental effects of ROS, osteoclast activation and subsequent bone resorption.[70,71] Therefore, we measured OPG expression by osteoblasts, distinguishing that the NTs regulated a mature protective microenvironment promoting similar OPG levels even under the uncontrolled DM condition. Interestingly, the activation of OPG after 21 days showed that osteoblasts could be downregulating the RANKL receptor, which is associated with a decreased late osteoclastogenesis and upregulated osteoblastogenesis considered a major determinant of bone mass.[72,73] The current OPG expression (the most important decoy receptor of RANKL) detected after 21 days suggested that the NTs affinity for osteoblasts maturation can conduct a prolonged bone growth process, a better bone remodeling cycle, and accelerated bone healing.[73,74] Thus, OPG modulatory expression may be the ultimate determinant of bone resorption and remodeling.[71] Considering the osteogenic markers of early and late bone formation with the OPG featured performance orchestrated by the NTs, we can note that the application of nanostructured surfaces can alleviate the cellular stress induced by dangerous DS conditions. The results of our current study point toward the potential and promising application of nanostructured surfaces for overcoming osteoblast-forming functionality under prejudicial metabolic conditions. However, more studies applying in vivo models and signaling pathways associated to cell adhesion are recommended to support our results.

Overall, our findings showed that NTs under crucial diabetes mellitus conditions in vitro can sustain the capability of osteoblast cell adhesion, proliferation, differentiation, and matrix mineralization, which was positively related to Ca deposition. However, the NTs significantly increased the expression of the regulating osteogenic markers Runx2, OCN, OPN, and OPG at different stages of maturation. The assumption that nanostructured surfaces have the property of inducing hydroxyapatite formation and subsequent osteoblast functionality under harmful conditions of disease opens a promising door for the future application of Ti_6Al_4V-NTs under diabetic conditions.

Conclusions

The present study showed that osteoblast bone-forming functionality performance by 70 nm NTs under DM conditions. Our work provides insight into part of the nanoscale-featured surface contact to ameliorate the harmful environmental effects of DS. Thus, suggesting that DS can initially suppress osteoblast adhesion on Ti_6Al_4V implant alloy and the nanotubular counterpart. Nonetheless, after five days of incubation, complete cellular recovery was stimulated by the NTs, proposing that cell-nanosurface interactions could overexpress the associated cell adhesion signaling pathways. Far more important is the striking differentiation, mineralization, and optimal osteogenic upregulation tailored by the NTs under long-term DS culture conditions. These positive outcomes of bone formation shed light on the nanostructured-configured materials to mitigate DM-induced bone dysfunction for clinical application in metabolically compromised patients.

Acknowledgments

The authors wish to thank the program No. A1-S-38368, "Proyecto Apoyado por el Fondo Sectorial de Investigación para la Educación" CB2017-2018, SEP-CONACYT, and Program 317330 FOP02 CONACYT, for financial support.

Disclosure

The authors report no conflicts of interest in this work.

References

1. Hu X-F, Wang L, Xiang G, Lei W, Feng Y-F. Angiogenesis impairment by the NADPH oxidase-triggered oxidative stress at the bone-implant interface: critical mechanisms and therapeutic targets for implant failure under hyperglycemic conditions in diabetes. *Acta Biomater*. 2018;73:470–487. doi:10.1016/j.actbio.2018.04.008
2. Facklam AL, Volpatti LR, Anderson DG. Biomaterials for personalized cell therapy. *Adv Mater*. 2020;32(13):1902005. doi:10.1002/adma.201902005
3. Aguado BA, Grim JC, Rosales AM, Watson-Capps JJ, Anseth KS. Engineering precision biomaterials for personalized medicine. *Sci Transl Med*. 2018;10(424):eaam8645. doi:10.1126/scitranslmed.aam8645
4. Peppas NA, Clegg JR. The challenge to improve the response of biomaterials to the physiological environment. *Regen Biomater*. 2016;3(2):67–71. doi:10.1093/rb/rbw012
5. Wagner J, Spille JH, Wiltfang J, Naujokat H. Systematic review on diabetes mellitus and dental implants: an update. *Int J Implant Dent*. 2022;8(1):1. doi:10.1186/s40729-021-00399-8
6. Ajami E, Mahno E, Mendes VC, Bell S, Moineddin R, Davies JE. Bone healing and the effect of implant surface topography on osteoconduction in hyperglycemia. *Acta Biomater*. 2014;10(1):394–405. doi:10.1016/j.actbio.2013.09.020
7. Oates TW, Huynh-Ba G, Vargas A, Alexander P, Feine J. A critical review of diabetes, glycemic control, and dental implant therapy. *Clin Oral Implants Res*. 2013;24(2):117–127. doi:10.1111/j.1600-0501.2011.02374.x
8. Moraschini V, Barboza ESP, Peixoto GA. The impact of diabetes on dental implant failure: a systematic review and meta-analysis. *Int J Oral Maxillofac Surg*. 2016;45(10):1237–1245. doi:10.1016/j.ijom.2016.05.019
9. Khader YS, Dauod AS, El-Qaderi SS, Alkafajei A, Batayha WQ. Periodontal status of diabetics compared with nondiabetics: a meta-analysis. *J Diabetes Complications*. 2006;20(1):59–68. doi:10.1016/j.jdiacomp.2005.05.006
10. Jiao H, Xiao E, Graves DT. Diabetes and its effect on bone and fracture healing. *Curr Osteoporos Rep*. 2015;13(5):327–335. doi:10.1007/s11914-015-0286-8
11. Ko KI, Sculean A, Graves DT. Diabetic wound healing in soft and hard oral tissues. *Transl Res*. 2021;236:72–86. doi:10.1016/j.trsl.2021.05.001
12. French D, Ofec R, Levin L. Long term clinical performance of 10 871 dental implants with up to 22 years of follow-up: a cohort study in 4247 patients. *Clin Implant Dent Relat Res*. 2021;23(3):289–297. doi:10.1111/cid.12994
13. Sghaireen MG, Alduraywish AA, Srivastava KC, et al. Comparative evaluation of dental implant failure among healthy and well-controlled diabetic patients—A 3-year retrospective study. *Int J Environ Res Public Health*. 2020;17(14):5253. doi:10.3390/ijerph17145253
14. Olson JW, Shernoff AF, Tarlow JL, Colwell JA, Scheetz JP, Bingham SF. Dental endosseous implant assessments in a type 2 diabetic population: a prospective study. *Int J Oral Maxillofac Implants*. 2000;15(6):811–818.
15. Spanheimer RG. Direct inhibition of collagen production in vitro by diabetic rat serum. *Metabolism*. 1988;37(5):479–485. doi:10.1016/0026-0495(88)90050-9

16. Deng X, Xu M, Shen M, Cheng J. Effects of type 2 diabetic serum on proliferation and osteogenic differentiation of mesenchymal stem cells. *J Diabetes Res*. 2018;2018:5765478. doi:10.1155/2018/5765478
17. Ceriello A, Giugliano D, Quatraro A, Russo PD, Lefèbvre PJ. Metabolic control may influence the increased superoxide generation in diabetic serum. *Diabetic Med*. 1991;8(6):540–542. doi:10.1111/j.1464-5491.1991.tb01647.x
18. Peliknov T, Kazdov L, Chvojkov R, Bae J. Serum phospholipid fatty acid composition and insulin action in type 2 diabetic patients. *Metabolism*. 2001;50(12):1472–1478. doi:10.1053/meta.2001.27195
19. Blake R, Trounce IA. Mitochondrial dysfunction and complications associated with diabetes. *Biochim Biophys Acta*. 2014;1840(4):1404–1412. doi:10.1016/j.bbagen.2013.11.007
20. Forbes JM, Thorburn DR. Mitochondrial dysfunction in diabetic kidney disease. *Nat Rev Nephrol*. 2018;14(5):291–312. doi:10.1038/nrneph.2018.9
21. Brammer KS, Frandsen CJ, Jin JS. TiO2 nanotubes for bone regeneration. *Trends Biotechnol*. 2012;30(6):315–322. doi:10.1016/j.tibtech.2012.02.005
22. Beltrán-Partida E, Moreno-Ulloa A, Valdez-Salas B, et al. Improved osteoblast and chondrocyte adhesion and viability by surface-modified Ti6Al4V alloy with anodized TiO2 nanotubes using a super-oxidative solution. *Materials*. 2015;8(3):867–883. doi:10.3390/ma8030867
23. Valdez-Salas B, Beltrán-Partida E, Nedev N, et al. Controlled antifungal behavior on Ti6Al4V nanostructured by chemical nanopatterning. *Mater Sci Eng C*. 2019;96:677–683. doi:10.1016/j.msec.2018.11.086
24. Gulati K, Zhang Y, Di P, Liu Y, Ivanovski S. Research to clinics: clinical translation considerations for anodized nano-engineered titanium implants. *ACS Biomater Sci Eng*. 2021;2021:34.
25. Civantos A, Martínez-Campos E, Ramos V, Elvira C, Gallardo A, Abarrategi A. Titanium coatings and surface modifications: toward clinically useful bioactive implants. *ACS Biomater Sci Eng*. 2017;3(7):1245–1261. doi:10.1021/acsbiomaterials.6b00604
26. Brammer KS, Oh S, Cobb CJ, Bjursten LM, Heyde H, Jin S. Improved bone-forming functionality on diameter-controlled TiO2 nanotube surface. *Acta Biomater*. 2009;5(8):3215–3223. doi:10.1016/j.actbio.2009.05.008
27. Jiang H, Ma X, Zhou W, et al. The effects of hierarchical micro/nano-structured titanium surface on osteoblast proliferation and differentiation under diabetic conditions. *Implant Dent*. 2017;26(2):263–269. doi:10.1097/ID.0000000000000576
28. Yang J, Zhang H, Chan SM, et al. TiO(2) nanotubes alleviate diabetes-induced osteogenetic inhibition. *Int J Nanomedicine*. 2020;15:3523–3537. doi:10.2147/IJN.S237008
29. Beltrán-Partida E, Valdéz-Salas B, Moreno-Ulloa A, et al. Improved in vitro angiogenic behavior on anodized titanium dioxide nanotubes. *J Nanobiotechnology*. 2017;15(1):10. doi:10.1186/s12951-017-0247-8
30. Beltrán-Partida E, Valdez-Salas B, Curiel-Álvarez M, Castillo-Uribe S, Escamilla A, Nedev N. Enhanced antifungal activity by disinfected titanium dioxide nanotubes via reduced nano-adhesion bonds. *Mater Sci Eng C*. 2017;76:59–65. doi:10.1016/j.msec.2017.02.153
31. Valdez-Salas B, Beltrán-Partida E, Curiel-Álvarez M, Guerra-Balcázar M, Arjona N. Crystallographic pattern mediates fungal nanoadhesion bond formation on titanium nanotubes. *ACS Omega*. 2021;6(24):15625–15636. doi:10.1021/acsomega.1c00475
32. Valdez-Salas B, Beltrán-Partida E, Castillo-Uribe S, et al. In vitro assessment of early bacterial activity on micro/nanostructured Ti6Al4V surfaces. *Molecules*. 2017;22(5):832. doi:10.3390/molecules22050832
33. Moseley KF, Doyle ME, Jan De Beur SM. Diabetic serum from older women increases adipogenic differentiation in mesenchymal stem cells. *Endocr Res*. 2018;43(3):155–165. doi:10.1080/07435800.2018.1441868
34. Li Y, Shrestha A, Zhang H, et al. Impact of diabetes mellitus simulations on bone cell behavior through in vitro models. *J Bone Miner Metab*. 2020;38(5):607–619. doi:10.1007/s00774-020-01101-5
35. Valdez-Salas B, Beltrán-Partida E. Feasibility of Using H3PO4/H2O2 in the synthesis of antimicrobial TiO2 nanoporous surfaces. *Bioinorg Chem Appl*. 2021;2021:6209094. doi:10.1155/2021/6209094
36. Valdez-Salas B, Beltrán-Partida E, Zlatev R, et al. Structure-activity relationship of diameter controlled Ag@Cu nanoparticles in broad-spectrum antibacterial mechanism. *Mater Sci Eng C*. 2021;119:111501. doi:10.1016/j.msec.2020.111501
37. Zhu S, Eldeeb MA, Pang SW. 3D nanoplasmonic biosensor for detection of filopodia in cells. *Lab Chip*. 2020;20(12):2188–2196. doi:10.1039/D0LC00173B
38. Gregory CA, Grady Gunn W, Peister A, Prockop DJ. An Alizarin red-based assay of mineralization by adherent cells in culture: comparison with cetylpyridinium chloride extraction. *Anal Biochem*. 2004;329(1):77–84. doi:10.1016/j.ab.2004.02.002
39. Zhang X, Li J, Wang X, et al. Effects of copper nanoparticles in porous TiO2 coatings on bacterial resistance and cytocompatibility of osteoblasts and endothelial cells. *Mater Sci Eng C*. 2018;82:110–120. doi:10.1016/j.msec.2017.08.061
40. Prasad S, Ehrensberger M, Gibson MP, Kim H, Monaco EA. Biomaterial properties of titanium in dentistry. *J Oral Biosci*. 2015;57(4):192–199. doi:10.1016/j.job.2015.08.001
41. Voltrova B, Hybasek V, Blahnova V, et al. Different diameters of titanium dioxide nanotubes modulate Saos-2 osteoblast-like cell adhesion and osteogenic differentiation and nanomechanical properties of the surface. *RSC Adv*. 2019;9(20):11341–11355. doi:10.1039/C9RA00761J
42. Lewis SR, Macey R, Lewis J, et al. Surgical interventions for treating extracapsular Hip fractures in older adults: a network meta-analysis. *Cochrane Database Syst Rev*. 2022;3(2):34.
43. Curtis DA, Lin G-H, Rajendran Y, Gessese T, Suryadevara J, Kapila YL. Treatment planning considerations in the older adult with periodontal disease. *Periodontol 2000*. 2021;87(1):157–165. doi:10.1111/prd.12383
44. Insua A, Monje A, Wang H-L, Miron RJ. Basis of bone metabolism around dental implants during osseointegration and peri-implant bone loss. *J Biomed Mater Res A*. 2017;105(7):2075–2089. doi:10.1002/jbm.a.36060
45. Mazare A, Totea G, Burnei C, Schmuki P, Demetrescu I, Ionita D. Corrosion, antibacterial activity and haemocompatibility of TiO2 nanotubes as a function of their annealing temperature. *Corros Sci*. 2016;103:215–222. doi:10.1016/j.corsci.2015.11.021
46. Yu W-Q, Qiu J, Xu L, Zhang F-Q. Corrosion behaviors of TiO 2 nanotube layers on titanium in Hank's solution. *Biomed Mater*. 2009;4(6):065012. doi:10.1088/1748-6041/4/6/065012
47. Wang Z, Wang X, Wang Y, Zhu Y, Liu X, Zhou Q. NanoZnO-modified titanium implants for enhanced anti-bacterial activity, osteogenesis and corrosion resistance. *J Nanobiotechnology*. 2021;19(1):353. doi:10.1186/s12951-021-01099-6
48. Hang R, Liu Y, Liu S, et al. Size-dependent corrosion behavior and cytocompatibility of Ni–Ti–O nanotubes prepared by anodization of biomedical NiTi alloy. *Corros Sci*. 2016;103:173–180. doi:10.1016/j.corsci.2015.11.016

49. Cho H-R, Choe H-C. Nanotube formation of Ti-6Al-4V alloy and its corrosion behavior. *Thin Solid Films*. 2022;751:139216. doi:10.1016/j.tsf.2022.139216
50. Yu Y, Shen X, Luo Z, et al. Osteogenesis potential of different titania nanotubes in oxidative stress microenvironment. *Biomaterials*. 2018;167:44–57. doi:10.1016/j.biomaterials.2018.03.024
51. Zheng N, Fitzpatrick V, Cheng R, Shi L, Kaplan DL, Yang C. Photoacoustic carbon nanotubes embedded silk scaffolds for neural stimulation and regeneration. *ACS Nano*. 2022;16(2):2292–2305. doi:10.1021/acsnano.1c08491
52. Mo R, Jiang T, Di J, Tai W, Gu Z. Emerging micro- and nanotechnology based synthetic approaches for insulin delivery. *Chem Soc Rev*. 2014;43(10):3595–3629. doi:10.1039/c3cs60436e
53. Hu Y, Cai K, Luo Z, et al. Regulation of the differentiation of mesenchymal stem cells in vitro and osteogenesis in vivo by microenvironmental modification of titanium alloy surfaces. *Biomaterials*. 2012;33(13):3515–3528. doi:10.1016/j.biomaterials.2012.01.040
54. Ding T, Kang W, Li J, Yu L, Ge S. An in situ tissue engineering scaffold with growth factors combining angiogenesis and osteoimmunomodulatory functions for advanced periodontal bone regeneration. *J Nanobiotechnology*. 2021;19(1):247. doi:10.1186/s12951-021-00992-4
55. Mata A, Geng Y, Henrikson KJ, et al. Bone regeneration mediated by biomimetic mineralization of a nanofiber matrix. *Biomaterials*. 2010;31(23):6004–6012. doi:10.1016/j.biomaterials.2010.04.013
56. Ma X-Y, Feng Y-F, Ma Z-S, et al. The promotion of osteointegration under diabetic conditions using chitosan/hydroxyapatite composite coating on porous titanium surfaces. *Biomaterials*. 2014;35(26):7259–7270. doi:10.1016/j.biomaterials.2014.05.028
57. Li X, Ma X-Y, Feng Y-F, et al. Osseointegration of chitosan coated porous titanium alloy implant by reactive oxygen species-mediated activation of the PI3K/AKT pathway under diabetic conditions. *Biomaterials*. 2015;36:44–54. doi:10.1016/j.biomaterials.2014.09.012
58. Hofbauer LC, Busse B, Eastell R, et al. Bone fragility in diabetes: novel concepts and clinical implications. *Lancet Diabetes Endocrinol*. 2022;10(3):207–220. doi:10.1016/S2213-8587(21)00347-8
59. Minagar S, Wang J, Berndt CC, Ivanova EP, Wen C. Cell response of anodized nanotubes on titanium and titanium alloys. *J Biomed Mater Res A*. 2013;101A(9):2726–2739. doi:10.1002/jbm.a.34575
60. Zhang H, Cooper LF, Zhang X, et al. Titanium nanotubes induce osteogenic differentiation through the FAK/RhoA/YAP cascade. *RSC Adv*. 2016;6(50):44062–44069. doi:10.1039/C6RA04002K
61. Ma X-Y, Feng Y-F, Wang T-S, et al. Involvement of FAK-mediated BMP-2/Smad pathway in mediating osteoblast adhesion and differentiation on nano-HA/chitosan composite coated titanium implant under diabetic conditions. *Biomater Sci*. 2018;6(1):225–238. doi:10.1039/C7BM00652G
62. Ma X-Y, Ma T-C, Feng Y-F, et al. Promotion of osteointegration under diabetic conditions by a silk fibroin coating on 3D-printed porous titanium implants via a ROS-mediated NF-κB pathway. *Biomed Mater*. 2021;16(3):035015. doi:10.1088/1748-605X/abaaa1
63. Franceschi RT, Iyer BS. Relationship between collagen synthesis and expression of the osteoblast phenotype in MC3T3-E1 cells. *J Bone Miner Res*. 1992;7(2):235–246. doi:10.1002/jbmr.5650070216
64. Franceschi RT, Iyer BS, Cui Y. Effects of ascorbic acid on collagen matrix formation and osteoblast differentiation in murine MC3T3-E1 cells. *J Bone Miner Res*. 1994;9(6):843–854. doi:10.1002/jbmr.5650090610
65. Xiao G, Cui Y, Ducy P, Karsenty G, Franceschi RT. Ascorbic acid-dependent activation of the osteocalcin promoter in MC3T3-E1 preosteoblasts: requirement for collagen matrix synthesis and the presence of an intact OSE2 sequence. *Mol Endocrinol*. 1997;11(8):1103–1113. doi:10.1210/mend.11.8.9955
66. Kawane T, Qin X, Jiang Q, et al. Runx2 is required for the proliferation of osteoblast progenitors and induces proliferation by regulating Fgfr2 and Fgfr3. *Sci Rep*. 2018;8(1):13551. doi:10.1038/s41598-018-31853-0
67. Teplyuk NM, Galindo M, Teplyuk VI, et al. Runx2 regulates g protein-coupled signaling pathways to control growth of osteoblast progenitors. *J Biol Chem*. 2008;283(41):27585–27597. doi:10.1074/jbc.M802453200
68. Yao H, Zou Y, Yang K, Yin L, Liu Y, Li R. TGFβ1 induces bone formation from BMP9-activated bone mesenchymal stem cells, with possible involvement of non-canonical pathways. *Int J Med Sci*. 2020;17(12):1692–1703. doi:10.7150/ijms.45786
69. Icer MA, Gezmen-Karadag M. The multiple functions and mechanisms of osteopontin. *Clin Biochem*. 2018;59:17–24. doi:10.1016/j.clinbiochem.2018.07.003
70. Ateeq H, Zia A, Husain Q, Khan MS, Ahmad M. Effect of inflammation on bones in diabetic patients with periodontitis via RANKL/OPG system-A review. *J Diabetes Metab Disord*. 2022;21(1):1003–1009. doi:10.1007/s40200-021-00960-7
71. Walsh MC, Choi Y. Biology of the RANKL–RANK–OPG system in immunity, bone, and beyond. *Front Immunol*. 2014;5. doi:10.3389/fimmu.2014.00511
72. Takegahara N, Kim H, Choi Y. RANKL biology. *Bone*. 2022;159:116353. doi:10.1016/j.bone.2022.116353
73. Boyce BF, Xing L. Biology of RANK, RANKL, and osteoprotegerin. *Arthritis Res Ther*. 2007;9(1):S1. doi:10.1186/ar2165
74. Fielding GA, Sarkar N, Vahabzadeh S, Bose S. Regulation of osteogenic markers at late stage of osteoblast differentiation in silicon and zinc doped porous TCP. *J Funct Biomater*. 2019;10(4):48. doi:10.3390/jfb10040048